ISIJ International, Vol. 58 (2018), No. 4, pp. 765–768

Development of Cube + Goss Texture in Electrical Steels and their Magnetic Properties

Hyunwoo MUN, Nam Hoe HEO* and Yangmo KOO

Graduate Institute of Ferrous Technology, Pohang University of Science and Technology (POSTECH), Pohang, 37673 Republic of Korea.

(*Received on November 7, 2017; accepted on December 22, 2017*)

After final annealing, magnetic properties of the electrical steel including the lowest bulk sulfur content are best, while those of the steel including the additional aluminum is worst. Such excellent magnetic properties in the former steel is due to the strong cube + Goss texture. The sulfur highly segregated at grain boundaries and the surface Al_2O_3 layer is detrimental to the selective growth of the cube and Goss grains, resulting in the smaller grain size and the final poor magnetic properties. The bulk content of sulfur and aluminum should, therefore, be decreased to obtain the strong cube + Goss texture.

KEY WORDS: AES; iron alloys; grain boundaries; recrystallization texture; segregation.

1. Introduction

Electrical steels are used for the core material of transformers and motors. The ideal electrical steel for the motor core is the steel composed of a (0 0 1) ⊥ ND texture which includes the [1 0 0] easiest magnetization direction. Such a (0 0 1) ⊥ ND textured electrical steel can be fabricated using the transformation of austenite to ferrite which is accompanied by the decarburization under a vacuum.[1–3] The cube texture develops generally during annealing after two-stage cold-rolling with the second-stage cold-rolling thickness reduction of about 50%.[1,2] Compared to the production process for conventional non-oriented electrical steels, the specific process needs a very long annealing time of about 10 h in developing the (0 0 1) ⊥ ND texture, due to the sluggish reaction of austenite to ferrite under a vacuum.

On the other hand, the surface energy of b.c.c. crystals increases in the order of (1 1 0), (0 0 1), (1 1 1) and other less densely packed planes.[4] In an electrical steel consisting of large (1 1 0) and (0 0 1) grains, the (1 1 0) grain grew at the expense of the (0 0 1) grain during vacuum annealing.[5–7] The situation was reversed during argon annealing, resulting in the growth of the (0 0 1) grain. Such a selective growth was explained in terms of the effect of oxygen which caused the lower surface energy of the (0 0 1) plane. The secondary recrystallization or the selective growth kinetics has been derived in strips where the average grain size is from one to two times the strip thickness.[8] In an annealing experiment under a hydrogen atmosphere with an additive of H_2S,[9,10] the (1 1 0) grain grew at the expense of the other (0 0 1) grain under a sulfur-free environment of hydrogen, but the (0 0 1) grain grew into the (1 1 0) grain under the hydrogen atmosphere containing H_2S. These results strongly indicate that some preferential adsorption of sulfur on the strip surface from the annealing atmosphere determines the selective growth between the (1 1 0) and (0 0 1) grains.

As mentioned above, the selective growth has simply been correlated to the annealing atmosphere without the consideration for effects of impurities in the bulk interior. Recently, it has been shown that in electrical steels the surface-energy-induced-selective growth is governed by the surface segregation of the sulfur itself which is contained in the bulk interior.[11,12]

It is the purpose of this study to investigate effects of bulk content of sulfur and aluminum on development of cube + Goss texture in electrical steels during final annealing in a pure hydrogen, using the conventional cold-rolling and annealing processes.

2. Experimental

Three kinds of Fe-3.1wt.%Si-0.1wt.%Mn electrical steel ingots, which contain 6 ppm S (6S), 20 ppm S (20S) and 6 ppm S and 0.8wt.%Al (6S8Al), were prepared using vacuum induction melting. The ingots were hot-rolled to 2.5 mm after the homogenization treatment at 1 150°C for 2 h. The hot-rolled plates were annealed at 1 050°C for 120 s.

Cold-rolled strips of 180 μm thickness were fabricated through a two-stage cold-rolling process including an intermediate annealing at 1 050°C for 120 s in the hydrogen of 5N purity at a flowing rate of 3 Liters H_2/min. The second stage cold-rolling thickness reduction was fixed at 50%. The conventional cold-rolling process, which is not the cross-rolling process, was used in this study. In the cold-rolling process, the thickness reduction per rolling pass was 100 μm. The cold-rolled strips with a dimension (10 mm in width and 100 mm in length parallel to the rolling direction) were

* Corresponding author: E-mail: nhheo@postech.ac.kr
DOI: http://dx.doi.org/10.2355/isijinternational.ISIJINT-2017-662

finally annealed at 1 000°C within 300 s under the same hydrogen atmosphere. After final annealing, stress relief annealing was carried out on the annealed strips at 800°C for 600 s under the same hydrogen atmosphere. All the annealing times include both the heating time to the heat treatment temperature and the holding time at the temperature. The heat treatments were performed using a tube furnace.

Magnetic properties of the annealed strips were measured in the rolling direction, using a single strip dc flux-meter. The magnetic properties in the transverse direction could not be measured, due to the dimensional limit of the cold-rolling mill and the tube furnace. ODFs (orientation distribution functions) were used for texture analyses. Changes in surface segregation of elements with final annealing time were investigated using an ion-sputtering technique in an AES (Auger electron spectroscope). All the differential peak heights of C_{275}, O_{510}, S_{153}, Si_{96}, Al_{1487} and Fe_{654} eV were normalized with the peak height, 100, of Fe_{654} eV. The primary beam energy was 3 keV and the sputtering rate was 14 Å of SiO_2/min. The ion-sputtering technique in the AES was also used to investigate the Al_2O_3 thickness formed on the surface of the 6S8Al steel strip during final annealing. The sputtering rate of this case was 44 Å of SiO_2/min.

3. Results and Discussion

Changes in magnetic properties of the 6S, 20S and 6S8Al steels and ODF with final annealing time are shown in **Fig. 1**. As shown in Fig. 1(a1), the magnetic induction of the steels decreases slightly until a critical time, after which it increases with further final annealing. Among the three steels, the magnetic induction (1.786 B_{50}T) of the 20S steel after annealing for 120 s is highest, while that (1.730 B_{50}T) of the 6S8Al steel is lowest. The core loss of Fig. 1(a2) decreases gradually with increasing annealing time. The core loss (1.288 $W_{15/50}$/kg) of the 6S steel after annealing for 120 s is lowest, while that (1.721 $W_{15/50}$/kg) of the 6S8Al steel is highest. Depending on the kind of motors, the highest magnetic induction of Fig. 1(a) or the lowest core loss may be chosen, if the steels are commercialized.

Figures 1(b)–1(d) show changes in ODF of the 6S, 20S and 6S8Al steels with final annealing time. After final annealing for 10 s, the 6S steel shows a strong Goss texture and a weak cube texture, as shown in Fig. 1(b). After final annealing for 120 s, the cube texture becomes stronger, while the Goss texture is changed to the strong Brass texture which is detrimental to magnetic properties. As shown in Fig. 1(c), such a trend is similar also in the 20S steel, although the summation of the core intensities is weaker than that of Fig. 1(b). In the 6S8Al steel, the summation of the core intensities is, as shown in Fig. 1(d), lowest among the three steels, and a noticeable (1 1 1) ⊥ ND texture is observed. That is, the Goss texture in the three steels develops during primary recrystallization rather than during grain growth. Therefore, the highest magnetic property of the 20S steel may be attributed to the moderate intensity of the (001) [100] and the (110) ⊥ ND texture which is close to not the Brass texture of Fig. 1(b) but the Goss texture.

Changes in grain size of the 6S, 20S and 6S8Al steels with final annealing time are shown in **Fig. 2**. Regardless of the final annealing time, the grain size of the 6S steel is largest, while that of the 20S steel is smallest. It is observed that the Goss grain colonies in the 6S steel of Fig. 2(a) are round, while those in the 20S steel of Fig. 2(b) are elongated, which may be related with different initial microstructures. As shown in **Fig. 3**, the cold-rolling textures of the 6S and 20S steels are similar, while the high-index textures are some different. In the two cold-rolled strips, the Goss texture is hardly observed, as shown in Fig. 3. As a result, the reason why the shape of the Goss grains in Figs. 2(a) and 2(b) is different is not still clear.

Ion-sputtering results obtained from the strip surface of the 6S, 20S and 6S8Al steels after final annealing are shown in **Fig. 4**. The maximum peak of sulfur observed during the ion-sputtering, which corresponds to each point of Fig. 4(a), was considered as the concentration of sulfur segregated at the free surface of the strip during final annealing. Oxygen and carbon peaks in ion-sputtering results of Fig. 4(b) are not considered, because they were adsorbed on the strip surface from air after final annealing. As shown in Fig. 4(a), the surface segregation concentration of sulfur in the 6S steel is little changed until the final annealing time of

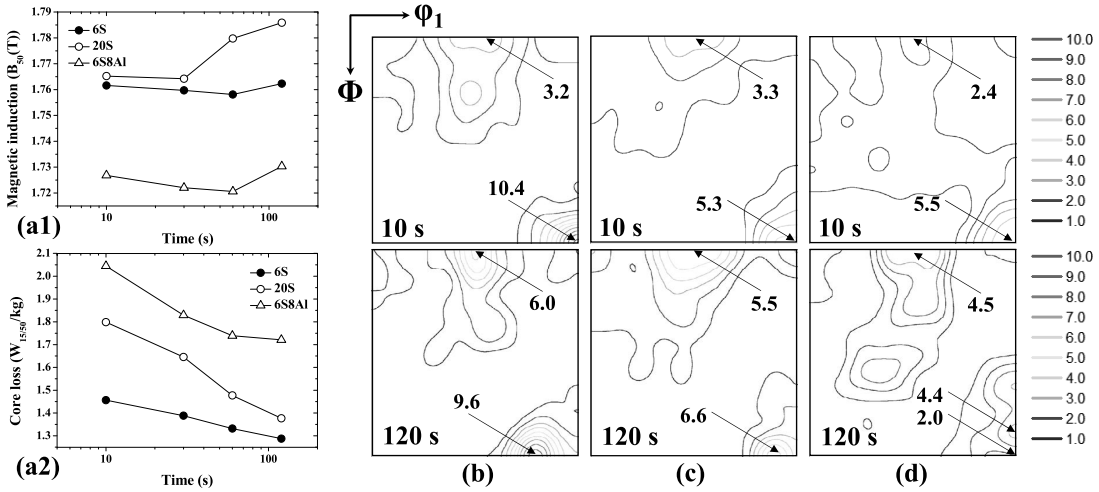

Fig. 1. Changes in magnetic properties of the 6S, 20S and 6S8Al steels and ODF with final annealing time: (a1) magnetic induction, (a2) core loss, (b) ODFs of the 6S steel, (c) ODFs of the 20S steel and (d) ODFs of the 6S8Al steel. φ_2=45°.

120 s, after which it decreases with further final annealing. Meanwhile, the surface segregation concentration of sulfur in the 20S steel shows a convex profile with final annealing time. The overall segregation concentration of the 20S steel is much higher than that of the 6S steel. This is because the equilibrium segregation concentration of an element increases with increasing bulk content of the element.[13] As shown in Fig. 4(b), the strip surface of the 6S8Al steel is covered with the Al_2O_3 layer which is formed by the oxidation reaction between Al and an extremely small amount of oxygen in the pure hydrogen of 5N purity. The thickness of the oxide layer simply calculated from the sputtering rate of 44 Å of SiO_2/min is about 2 200 Å. The investigation for the segregation behavior of sulfur failed in the 6S8Al steel due to the thick Al_2O_3 layer.

It has been reported that the magnetic induction (B_{50}(T)) of non-oriented electrical steels decreases gradually with increasing grain size in the range of grain sizes larger than 50 μm, while the core loss ($Watt_{15/50}$/kg) increases with increasing grain size in the range of grain sizes larger than 150 μm.[14] Following the previous research,[14] the slight decrease in magnetic induction until the critical time of Fig. 1(a1) is due to the increase in grain size. The increase in magnetic induction after the critical time of Fig. 1(a1) can be mainly attributed to the development of the cube + Goss texture of Figs. 1(b)–1(d) which is favorable for the easy magnetization. However, there is a controversy against the previous research where the magnetic induction increases with

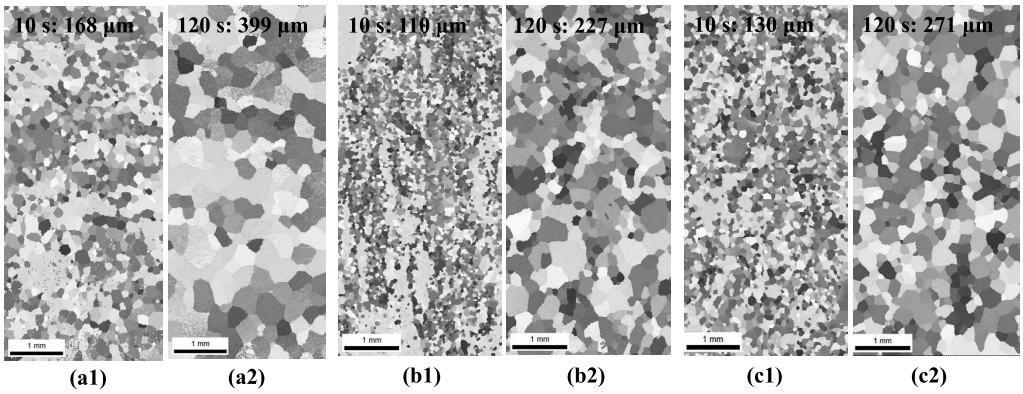

Fig. 2. Changes in grain size of the 6S, 20S and 6S8Al steels with final annealing time which are obtained from the EBSD analyses: (a) 6S, (b) 20S and (c) 6S8Al.

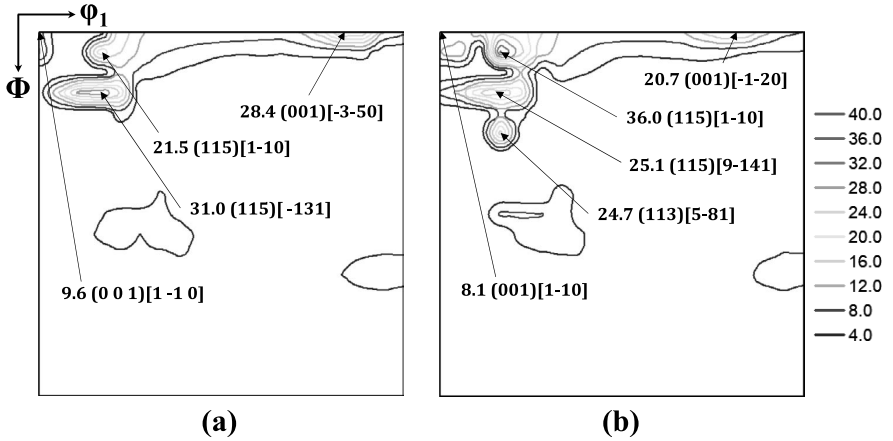

Fig. 3. Changes in cold-rolling texture with composition: (a) 6S and (b) 20S steels. φ_2=45°.

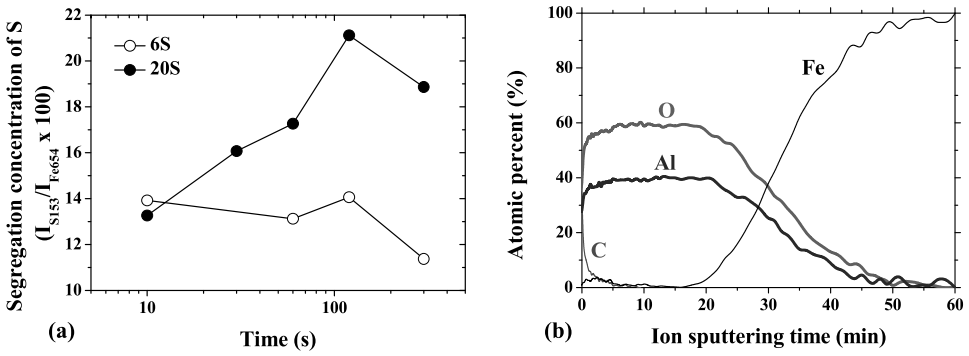

Fig. 4. Ion-sputtering results obtained from the strip surface of the 6S, 20S and 6S8Al steels after final annealing: (a) changes in surface segregation concentration of sulfur with final annealing time and (b) ion-sputtering results showing the Al_2O_3 layer formed on the strip of the 6S8Al steel after final annealing for 300 s.

increasing grain size in the grain size range of about 1 μm to 1 mm.[15] On the other hand, the core loss in non-oriented electrical steels decreases generally with increasing average grain size below an upper limit of the average grain size. Because the upper limit depends on composition, microstructure and processing parameters, there is no fixed upper limit which is generally valid for all cases.[16,17] Therefore, the abrupt decrease in core loss of Fig. 1(a2) with increasing final annealing time is due to the increase of grain size as well as the development of the strong cube + Goss texture.

The convex profile of sulfur during annealing[12] governs the selective growth of (1 1 0), (0 0 1) and (1 1 1) grains. The previous research for grain-oriented electrical steels[18,19] has shown that a high heating rate is favorable for the formation of the initial Goss texture during final annealing due to the selective growth of the Goss grains under the low surface segregation concentration of sulfur. The strong Goss texture of Figs. 1(b)–1(d) after final annealing for 10 s may be attributed to the high heating rate effect. Together with the Goss texture little changed, the occurrence of the strong cube texture after final annealing for 120 s is due to the selective growth of the cube grains under an appropriate surface segregation concentration of sulfur which is shown in Fig. 4(a). Among the (0 0 1) $\perp$ ND textures, the formation mechanism of the cube texture which is accompanied by the two-stage cold-rolling process is not still understood. Further study is needed in this direction.

As shown in Figs. 2(a) and 2(b), the smaller grain size in the 20S steel than the 6S steel is attributed to the strong grain boundary pinning effect of the sulfur highly segregated at the grain boundaries.[12,20,21] Generally, the thick surface Al_2O_3 layer of Fig. 4(b) penetrates along grain boundaries, which can also inhibit the movement of the grain boundaries. Additionally, the surface Al_2O_3 layer may interfere the H_2S reaction between the surface-segregated sulfur and the surrounding hydrogen, resulting in the increase in segregation concentration of sulfur at the strip surface and the grain boundaries. Therefore, the smaller grain size (Fig. 1(c)) in the 6S8Al steel than the 6S steel and the poor magnetic properties (Fig. 1(a)) are attributed to such roles of the Al_2O_3 layer.

In conventional non-oriented electrical steels, Al of 0.2–0.7 wt.% has been added to decrease the core loss.[22,23] **Figure 5** shows the comparison between magnetic properties of the 6S steel and the conventional non-oriented electrical steels.[24] At the same 350 μm thickness of Fig. 5, the decrease in core loss of the JFE steels with increasing Al content suffers from the decrease in magnetic induction. It is interesting that, although the strip thickness has been reduced to lower the core loss, the minimum core loss in the JFE steels is obtained from the strip of not 200 but 350 μm thickness. The conventional non-oriented electrical steels of 350 μm thickness show the best magnetic properties (B_{50} of 1.65 Tesla and the core loss of 2.05 $Watt_{15/50}$/kg). As shown Fig. 5, the magnetic properties (B_{50} of 1.762 Tesla and the core loss of 1.288 $Watt_{15/50}$/kg) of the 6S steel are much more excellent than those of the conventional non-oriented electrical steels.

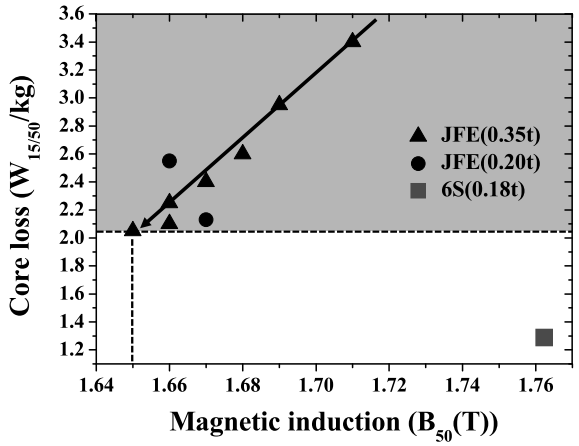

Fig. 5. The comparison between magnetic properties of the 6S steel and the conventional non-oriented electrical steels. The magnetic properties of the 6S steel were obtained from the strip finally annealed at 1 000°C for 120 s.

4. Conclusions

Effects of bulk content of sulfur and aluminum on development of cube + Goss texture in electrical steels have been investigated, and the results are as follows.

(1) The electrical steel including the lowest bulk sulfur content shows the best magnetic properties after final annealing. Such excellent magnetic properties in the former steel is due to the strong cube + Goss texture.

(2) The electrical steels including aluminum and the high bulk content of sulfur show the poor magnetic properties.

(3) The sulfur highly segregated at grain boundaries and the Al_2O_3 layer formed at the surface inhibit the selective growth of the cube and Goss grains, resulting in the smaller grain size and the final poor magnetic properties.

(4) The bulk content of sulfur and aluminum should, therefore, be decreased to obtain high magnetic properties.

REFERENCES

1) T. Tomida and S. Uenoya: *IEEE Trans. Magn.*, **37** (2001), 2318.
2) T. Tomida, S. Uenoya and N. Sano: *Mater. Trans.*, **44** (2003), 1106.
3) T. Tomida: *Mater. Trans.*, **44** (2003), 1096.
4) J. Friedel, B. D. Cullity and C. Crussard: *Acta Metall.*, **1** (1953), 79.
5) J. L. Walter and C. G. Dunn: *Acta Metall.*, **8** (1960), 497.
6) J. L. Walter and C. G. Dunn: *Trans. Am. Inst. Min. Eng.*, **215** (1959), 465.
7) J. L. Walter and C. G. Dunn: *Trans. Am. Inst. Min. Eng.*, **218** (1960), 1033.
8) K. Foster, J. J. Kramer and G. W. Wiener: *Trans. Am. Inst. Min. Eng.*, **227** (1963), 185.
9) D. Köhler: *J. Appl. Phys.*, **31** (1960), 408S.
10) J. J. Kramer: *Metall. Trans. A*, **23** (1992), 1987.
11) K. H. Chai, N. H. Heo, J. G. Na, I. K. Song and S. R. Lee: *IEEE Trans. Magn.*, **37** (2001), 2325.
12) N. H. Heo, K. H. Chai and J. G. Na: *Acta Mater.*, **48** (2000), 2901.
13) D. McLean: Grain Boundaries in Metals, Oxford University Press, London, (1957), 118.
14) M. Shiozaki and Y. Kurosaki: *J. Mater. Eng.*, **11** (1989), 37.
15) G. Herzer: *IEEE Trans. Magn.*, **26** (1990), 1397.
16) M. F. Littmann: *J. Appl. Phys.*, **38** (1967), 1104.
17) M. F. de Campos, J. C. Teixeira and F. J. G. Landgraf: *J. Magn. Magn. Mater.*, **301** (2006), 94.
18) N. H. Heo: *Metall. Mater. Trans. A*, **36** (2005), 3251.
19) N. H. Heo: *Mater. Lett.*, **59** (2005), 2170.
20) K. Lücke and K. Detert: *Acta Metall.*, **5** (1957), 628.
21) J. W. Cahn: *Acta Metall.*, **10** (1962), 789.
22) E. P. Wohlfarth: Ferromagnetic Materials, Vol. 2, North-Holland Publishing Company, Amsterdam, New York, (1980), 35.
23) E. T. Stephenson: *J. Appl. Phys.*, **55** (1984), 2142.
24) JFE: Electrical Steel Sheets JFE G-CORE, JFE N-CORE, http://www.jfe-steel.co.jp/en/products/electrical/catalog/f1e-001.pdf, (accessed 2017-05-21).